

Interpretation of hot and dense absorption spectra of a near-local-thermodynamic-equilibrium plasma by the super-transition-array method

A. Bar-Shalom and J. Oreg

Nuclear Research Center, Negev, P.O. Box 9001, Beer-Sheva, Israel 84190

J. F. Seely, U. Feldman, and C. M. Brown

E. O. Hulburt Center for Space Research, Naval Research Laboratory, Washington, D.C. 20375-5352

B. A. Hammel, R. W. Lee, and C. A. Back

Lawrence Livermore National Laboratory, Livermore, California 94550

(Received 30 May 1995)

The super-transition-array model is shown to be a very convenient tool for the interpretation of near-local-thermodynamic-equilibrium hot and dense plasmas. Specifically, we interpret here the absorption spectra of the CH-Ni-CH foil experiment performed at Lawrence Livermore National Laboratory using the backlighter technique. In this experiment a laminar foil composed of 200-Å Ni with 1000-Å CH on both sides was radiatively heated by the x-ray continuum from a nearby gold plasma and was backlit by the x-ray continuum from a distant gold plasma that could be time delayed with respect to the heating pulse. This setup was designed to achieve a uniform density and heating of the Ni middle layer. It is found that the Ni absorption features depend very weakly on the density of the foil but are quite sensitive to the foil temperature. Remarkably good agreement between the theory and the experiment is obtained for the Ni $2p$ - $3d$ spectrum. The detailed features indicate that the plasma temperature is confined to a narrow range between 14 and 18 eV, demonstrating that the foil design, aiming to create a homogeneous Ni plasma, was successful. These results represent an alternative temperature diagnostic for high- Z plasma.

PACS number(s): 52.70.-m

I. INTRODUCTION

In this work we apply the super-transition-array (STA) method [1–5] to interpret the absorption spectra obtained from hot and dense plasmas in the near-local-thermodynamic-equilibrium (LTE) regime, created by irradiation of matter by x-ray emission of a gold plasma. For relatively high- Z materials (e.g., Ni) such plasmas contain a huge number of transitions even when LTE conditions do not exactly hold, and the spectrum has many unresolved structures. The application of the collisional radiative model in these cases is a tremendous effort if possible at all. It is shown that the STA model, though based on LTE conditions, is a very convenient tool for the interpretation of such plasmas. For given temperature and density, it produces the exact wavelengths and widths of *all* the contributing clusters, including the individual linewidths and the entire cluster widths constructed from the many overlapping lines. The deviation in the intensities reveals the degree of departure from LTE conditions.

Specifically, we interpret here the absorption spectrum obtained in the CH-Ni-CH foil experiments performed at Livermore [6,7]. In these experiments a laminar foil composed of 200-Å Ni with 1000-Å CH on both sides was radiatively heated by the x-ray continuum from a nearby gold plasma, and was backlit by the x-ray continuum from a distant gold plasma that could be time de-

layed with respect to the heating pulse [8]. The tamped CH-Ni-CH foil was designed to achieve a uniform density and heating of the Ni middle layer. As we shall see, the Ni absorption features depend very weakly on the density of the foil but are quite sensitive to the foil temperature. The comparison between theory and experiment shows remarkable agreement for the Ni $2p$ - $3d$ spectrum. The detailed features in this region indicate that the plasma temperature is indeed confined to a narrow range between 14 and 18 eV. These results represent a temperature diagnostic for high- Z plasmas. In Sec. II we briefly review the STA model and the experimental setup. In Sec. III we compare the experimental and STA theoretical results. A discussion and summary are given in Sec. IV.

II. REVIEW OF THE THEORY AND EXPERIMENT

A. STA model

The most complex contribution to the spectrum emitted from hot and dense plasmas arises from the huge number of bound-bound and bound-free transitions. Unresolved clusters of many neighboring partially overlapping transition lines are created, constructing a complex intensity profile. The STA model reveals this complicated structure by a convergence procedure which increases the resolution of the calculated spectrum, until the re-

quired accuracy is achieved. Particularly, in each step the entire bulk of transitions is divided into groups G of neighboring lines, and each group is described as a Gaussian having the exact group moments, i.e., total intensity, average energy, and variance. The resolution is thus increased with the number of groups.

Specifically, the total spectrum can be written as

$$S(E) = \sum_G S_G(E), \quad (1)$$

where

$$S_G(E) = \sum_{i,j \in G} N_i w_{ij} P_{ij}(E - E_{ij}). \quad (2)$$

In Eq. (2) the summation is over all the transitions $i \rightarrow j$ in G , where i and j indicate the corresponding initial and final levels. N_i is the population of the initial level, w_{ij} is the transition probability, and P_{ij} is the corresponding line shape centered on the transition average energy E_{ij} .

For normalized symmetric line profiles, the group moments are the following:

intensity

$$I_G \equiv \int S_G(E) dE = \sum_{i,j \in G} N_i w_{ij}, \quad (3)$$

average energy

$$E_G \equiv \frac{\int S_G(E) E dE}{I_G} = \frac{\sum_{i,j \in G} N_i w_{ij} E_{ij}}{I_G}, \quad (4)$$

and variance

$$(\Delta E_G)^2 \equiv \frac{\int S_G(E) (E - E_G)^2 dE}{I_G} = \Delta_G^2 + \Delta_P^2, \quad (5)$$

where

$$\Delta_G^2 = \frac{\sum_{i,j \in G} N_i w_{ij} (E_{ij} - E_G)^2}{I_G}, \quad (6)$$

and

$$\Delta_P^2 = \int P(E - \bar{E})(E - \bar{E})^2 dE \quad (7)$$

is the variance of the individual line shape, assumed to be equal for all lines in group G .

The central achievement of STA theory is the ability to obtain, under certain conditions detailed below, analytical formulas for the moments, bypassing the impractical need to account for the huge number of transitions one by one [1,5]. The only two assumptions made are that (1) the plasma is in LTE conditions, yielding Boltzmann populations N_i ; and (2) The configuration widths are smaller than kT .

In addition, the definition of STA groups described below has two advantages [1,5]: (1) it enables one, using these assumptions, to derive analytic expressions for the group moments; and (2) it allows a group splitting strategy which speeds up the convergence. For bound free transitions the final level j belong to the continuum, and the moments of G are obtained by integration over the continuum [2,3].

In order to account for the non-Gaussian nature of P , we first construct a Gaussian from the moments I_G , E_G ,

and Δ_G ,

$$\Gamma(E - E_G) = \frac{I_G}{\sqrt{2\pi}\Delta_G} \exp \left[-\frac{1}{2} \left(\frac{E - E_G}{\Delta_G} \right)^2 \right], \quad (8)$$

and then construct the spectrum $S_G(E)$ by the convolution with the individual line shape

$$S_G(E) \equiv \int \Gamma(E - E_G) P(E - E) dE \quad (9)$$

having the same moments as the original spectrum of G defined by Eq. (2).

In order to complete this brief description of the theory, we now define the STA groups. A STA group (termed STA) is the collection of all transitions between two superconfigurations. A superconfiguration Ξ is a collection of ordinary configurations defined symbolically by the product over supershells σ ,

$$\Xi \equiv \prod_{\sigma} \sigma^{Q_{\sigma}}. \quad (10)$$

A supershell, in turn, is the union of energetically adjacent ordinary atomic subshells $s \equiv j_s \equiv n_s l_s j_s$. In Eq. (10), the superconfigurations are constructed by distributing the Q_{σ} electrons occupying the supershell σ among the subshells s in all possible ways subject to $\{\sum_{s \in \sigma} q_s = Q_{\sigma}\}$:

$$\sigma^{Q_{\sigma}} \equiv \sum_{\{\sum_{s \in \sigma} q_s = Q_{\sigma}\}} \prod_s j_s^{q_s}. \quad (11)$$

Clearly each partition of Q_{σ} is an ordinary configuration. The transitions between two configurations constitute an unresolved transition array (UTA) [9,10], and a STA is thus a collection of energetically near UTA's.

The convergence procedure mentioned above splits supershells into smaller supershells according to their energy spread. For each superconfiguration in its turn, at each step, supershells that give rise to relatively well-separated configurations, are preferentially split. The detailed structure of the spectrum is thus gradually revealed, yielding a converging spectrum. This procedure converges to the UTA spectra where each UTA is completely unresolved.

It is appropriate to collect separately all STA's belonging to a specific one electron jump $j_{\alpha} \rightarrow j_{\beta}$, e.g., $2p_{3/2} \rightarrow 3d_{5/2}$, which fall in the same region. This characterization will be used in comparison with the experiment given in Sec. II B.

Finally, three essential points should be emphasized here.

(1) The convergence procedure also allows the use of first order energies in the Boltzmann factor for the level configurations [2,3].

(2) Orbital relaxation is applied by taking different potentials for different superconfigurations [2,3]. This relaxation is carried out for different STA's as well as for the lower and upper superconfigurations of the same STA. As we shall see, this orbital relaxation significantly improves the agreement between the calculated and experimental spectra.

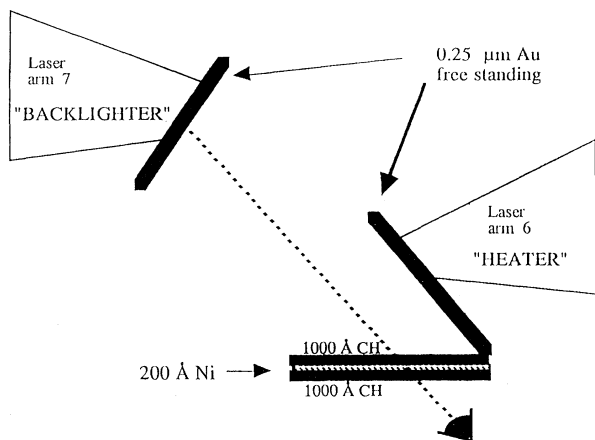
(3) The STA model was extended [4] to include the im-

portant part of the configuration interaction, i.e., the interaction between j - j configurations belonging to the same LS configuration. As will be seen below, these developments significantly improve the agreement with experimental results. The STA code is a very convenient tool for spectral diagnostics. Given the material density and temperature, it produces the entire spectra in a single run. It allows fast identification of the various arrays and lines. The deviation in intensities may help to understand the experimental conditions, i.e., the degree of departure from LTE conditions or the occurrence of stimulated emission as detailed below.

B. Experiment

The experiment and its motivation were discussed in detail in Refs. 6 and 7. A brief summary of the experiment is given below for convenience.

The experimental setup is shown schematically in Fig. 1. Two arms of the NOVA laser were used. One irradiates a thin gold foil emitting, in turn, x rays which heat the CH/Ni/CH foil target. The second laser arm heats a second gold foil which emits an x ray directly on the already heated target. The spectrally resolved absorption of this backlight continuum is detected at the back of the target. The tamped CH-Ni-CH foil, composed of 200-Å Ni with 1000-Å CH on both sides, was designed to achieve a uniform density and heating of the middle layer. The carbon on both sides of the Ni, on the other hand, blows off and is expected to have a much wider range of temperature and density. The spectrum in the wavelength range 6–100 Å of the backlighter continuum transmitted through the radiatively heated foil was photographically recorded by a high-resolution grazing in-



The Experimental Setup

FIG. 1. The experimental setup: two arms of the NOVA laser are used. One irradiates a thin gold foil, emitting, in turn, x rays which heat the CH-Ni-CH foil target. The second laser arm heats a second gold foil which emits an x ray directly on the already heated target. The absorption of this second laser light vs frequency is detected at the back of the target.

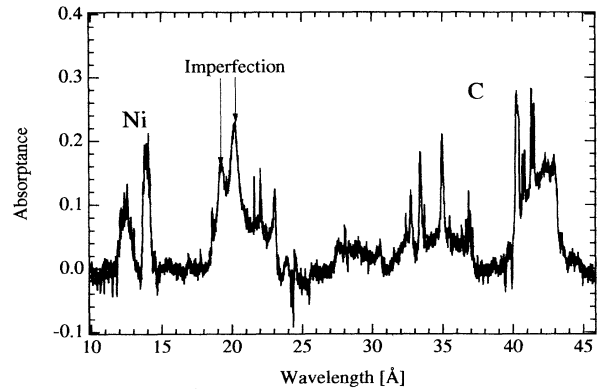


FIG. 2. The experimental spectrum includes contributions from C II to C V in the wavelength range 32–42 Å and a few ionization stages of Ni at wavelengths 12–14 Å. The features near 22 Å are of oxygen existing in the plastic layer not considered in this work. The features at 19–21 Å are imperfections in the photographic emulsion that appear in this particular lineout.

cidence spectrograph.

The Ni absorption features depend very weakly on the density of the foil, but are quite sensitive to the foil temperature. We will show that Ni transitions of the type $2p$ - $3d$ originate from plasma of temperatures in the narrow range 14–18 eV, indicating that a homogeneous Ni plasma was indeed achieved. This analysis represents an alternative temperature diagnostic for high- Z plasmas. In comparing the experimental and theoretical results, we have found deviations in intensity ratios between transition arrays originating from the same initial states. This is attributed to stimulated emission from highly populated final levels due to the photon flux from a much higher temperature gold plasma.

The experimental spectrum presented in Fig. 2 includes contributions from C II to C V in the wavelength range 32–42 Å and a few ionization stages of Ni at wavelengths 12–14 Å. The identification of the spectral features and the calibration of the photographic plates were discussed in Ref. [6]. The cold Ni L edge at 14.5 Å is absent in the spectrum. The features near 22 Å (the cold edge at 23.3 Å) are of oxygen existing in the plastic layer not considered in this work. The features at 19–21 Å are imperfections in the photographic emulsion that appear in this particular lineout.

III. INTERPRETATION OF THE SPECTRA BY THE STA MODEL

The experimental *absorption* spectrum is related to the absorption coefficient $\sigma(\lambda, \rho, T)$ by

$$A(\lambda) = (1 - e^{-\sigma(\lambda)\rho\Delta x}), \quad (12)$$

where $\rho\Delta x$ is the plasma depth, estimated to be $2 \cdot 10^{-5}$ g/cm² in our experiment. The STA model described in Sec. II calculates $S = \sigma\rho$ of Eq. (1) from which we obtain $A(\lambda)$.

The experimental and theoretical spectra are shown in Figs. 3–5. We have found that the resolved structures

originate from the superconfigurations

$$\Xi = (1s^2 2s^2 2p^6)(3s 3p_{1/2} 3p_{3/2} 3d_{3/2} 3d_{5/2})^N \times (4s 4p_{1/2} \dots)^M, \quad (13)$$

where $N = 8-11$ and the M 's (mainly between $M=0$ and 2) are not resolved. The observed transition arrays belong to one electron jumps $2p \rightarrow nd$ ($2p_{1/2} \rightarrow nd_{3/2} + 2p_{3/2} \rightarrow nd_{3/2} + 2p_{3/2} \rightarrow nd_{5/2}$) with $n=3, 4$, and 5.

In Fig. 3 we examine the $2p \rightarrow 3d$ spectra. Four spectra are shown for four temperatures from 10 to 22 eV. In Fig. 3(a) it is seen immediately that the calculated spectra of the two extreme temperatures (belonging to $T=10$ and 22 eV) extend beyond the experimental spectral structure. This limits the temperature spread to about 4 eV only ($T=14-18$ eV) as seen in Fig. 3(b). We have found that due to its narrow range the contribution of the entire continuous temperature profile can be well represented by

the two limiting values ($T=14$ and 18 eV). The addition of intermediate temperatures alters the spectrum only slightly.

In Figs. 4(a) and 4(b) the two temperature spectra of $2p \rightarrow 3d$ are shown. The "total" curve is the "best" combination of the two temperatures (40% $T=14$ eV + 60% $T=18$ eV). In Fig. 4(a) we present the theoretical result without configuration interaction (CI) [11], whereas Fig. 4(b) includes CI in agreement with the experiment. In Fig. 4(b) we also present a complete identification of all the resolved arrays using the compact notation N^- and N^+ for arrays $2p_{1/2} \rightarrow nd_{3/2}$ and $2p_{3/2} \rightarrow nd_{5/2}$, respectively. As expected, array $2p_{3/2} \rightarrow nd_{3/2}$ is negligibly weak, and only N^- and N^+ are observed. The agreement is strikingly good, and all arrays $N=9-11$ (denoted by $9^\pm-11^\pm$) are identified. In pure $j-j$ coupling (without CI) the ratio between the + and - transitions is in favor of the + transitions, and the departure from $j-j$ already seen in Fig. 3(a). It should be emphasized here that this excellent agreement was obtained only after improving the orbital relaxation, using a sufficient number of opti-

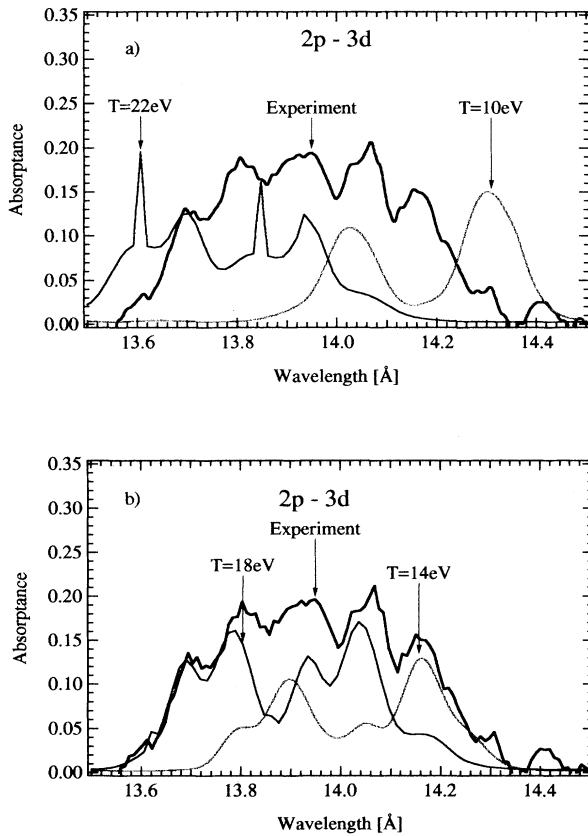


FIG. 3. Comparison between the theoretical and the experimental $2p \rightarrow 3d$ spectrum. (a) Two temperature (10 and 22 eV) spectra beyond the experimental limit. (b) The theoretical spectra of the temperature bounds (14 and 18 eV) reproducing the experimental spectrum.

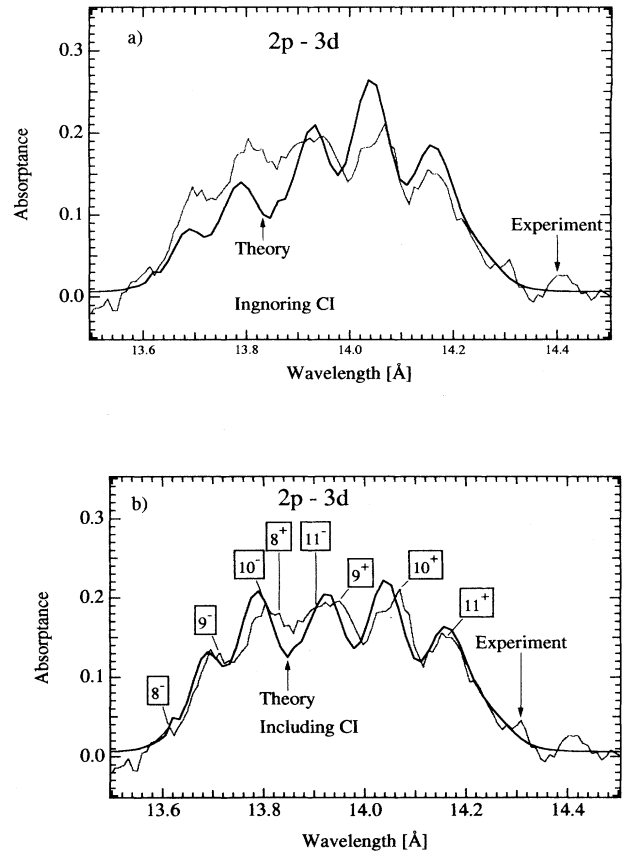


FIG. 4. The total two temperature (40% $T=14$ eV + 60% $T=18$ eV) spectra of $2p \rightarrow 3d$: (a) without CI, and (b) with CI. N^+ and N^- indicate the $2p_{1/2} \rightarrow nd_{3/2}$ and $2p_{3/2} \rightarrow nd_{5/2}$ transitions, respectively.

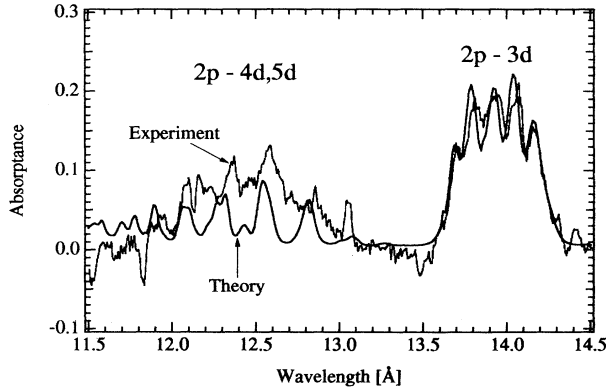


FIG. 5. The complete Ni LTE spectrum at $T=14\text{ eV}+18\text{ eV}$ and density 0.01 g/cc .

mized potentials for both initial and final superconfigurations. This comparison thus demonstrates the importance of both orbital relaxation and CI for the interpretation of plasma experiments.

The fact that the $2p\text{-}3d$ features are modeled so well is the most interesting result of this work, indicating that only three Ni ionization states contribute to this spectrum, and that the temperature range is extremely narrow ($14\text{--}18\text{ eV}$). These results, together with the absence of the Ni cold L edge at 14.5 eV , imply that the Ni plasma was uniformly heated by the x-ray continuum without large temperature gradients. This confirms the success of the foil design to avoid fast expansion of the middle layer and to allow a uniform heating.

In Fig. 5 the complete two temperature ($40\% T=14\text{ eV}+60\% T=18\text{ eV}$) Ni spectrum is presented. The comparison between the experiment and STA are not so good for the transitions $2p\rightarrow 4d, 5d$. Whereas shifts in wavelength can be improved by better optimization of the potential, we can see significant deviations in intensity ratios

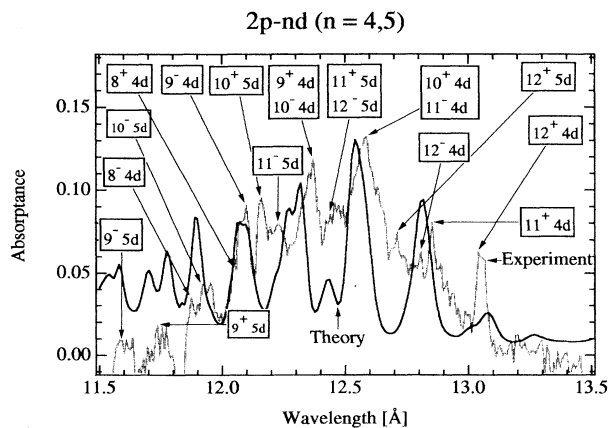


FIG. 6. Identification of the $2p\rightarrow 4d, 5d$ transitions. (N, nl) indicates the $2p\rightarrow nl$ one-electron jump origination from the bulk of superconfigurations denoted in the text by N , $(N, M$; summed over all M) of Eq. (13).

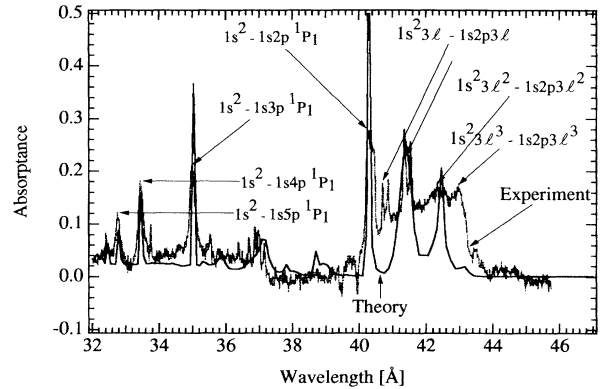


FIG. 7. Identification of the carbon LTE spectrum at $T=14\text{ eV}+18\text{ eV}$ and density 0.01 g/cc . The noisy and smooth lines are the experimental and theoretical results, respectively.

between transition arrays $2p\rightarrow 4d, 5d$ and $2p\rightarrow 3d$. These deviations cannot be attributed to a departure from LTE *absorption* since all these arrays originate from the same initial states. Departure from the LTE may affect these intensity ratios only through stimulated emission. Whereas under LTE conditions stimulated emission is obtained by simply multiplying the absorption spectra by the Planck function at the plasma temperature (in our case $14\text{ eV} < T < 18\text{ eV}$), a non-LTE effect can originate here from the *photon flux from the much higher temperature (keV) gold plasma (in the spectral region of these arrays)*. The discrepancy in the intensities can therefore be explained as follows: We could adjust the plasma depth Δx of Eq. (12) to fit the total intensity at the $2p\rightarrow 4d, 5d$ region. In such a normalization the $2p\text{-}3d$ calculated spectrum will still follow the detailed structure of the experimental spectrum but will be globally intensified. The lower experimental intensity in this region can now be attributed to the *non-LTE stimulated emission from the highly populated final levels of the $2p\text{-}3d$ array due to the photon flux from the much higher temperature (keV) gold and to the strong $2p\text{-}3d$ transition probability (relative to the $2p\rightarrow 4d, 5d$)*. A more quantitative explanation can be obtained by solving the detailed collisional radiative model. Such a calculation is beyond the scope of the present work.

In spite of these deviations, almost all the unresolved arrays of the transitions $(8^{\pm}, 4d)$ $(12^{\pm}, 4d)$ and $(9^{\pm}, 12^{\pm}, 5d)$ could be identified, as is specified in Fig. 6. The carbon on both sides of the Ni layer blows off, and is expected to have a much higher range of temperatures and density. It is thus not surprising that the modeling of carbon is not so good. The results for carbon are presented in Fig. 7. Again the strongest features could be identified in spite of the temperature spread which could not be accounted for accurately in the calculation.

IV. SUMMARY AND DISCUSSION

In this work we have demonstrated how the STA model can be used for the interpretation of near-LTE plasma

experiments. We have shown that for sufficiently relaxed orbitals the wavelengths of the various arrays in the entire spectral region are accurately calculated. The deviations from the LTE level populations may, in general, change the entire spectrum. Dominant LTE arrays may vanish and others may become significant. In this case a detailed collisional radiative model must be solved to obtain the level populations and the resulting array intensities. This is an enormous task. In contrast the STA model is a very simple tool, yielding the entire spectrum in a single run and allowing fast identification of all resolved arrays and lines. Of course STA spectra can be used quantitatively only if the departure from the LTE is

not too large so that the LTE features are still recognizable. In the present experiments we have distinguished only small non-LTE effects. The remarkable reconstruction of the experimental $2p\text{-}3d$ spectra by the theory with only two temperatures in a range of only 4 eV confirmed the success of the foil design aiming at homogeneous plasma in both density and temperature. The deviations in relative intensities of $2p\rightarrow nd$ arrays, between transitions with $n=4$ and 5 and with $n=3$, are attributed to spontaneous and stimulated emission from highly populated final levels due to the photon flux from the much higher temperature gold plasma. This work introduces an alternative temperature diagnostic for high-Z plasma.

-
- [1] A. Bar-Shalom, J. Oreg, W. H. Goldstein, D. Shvarts, and A. Zigler, *Phys. Rev. A* **40**, 3183 (1989).
- [2] A. Bar-Shalom, J. Oreg, and W. H. Goldstein, in *Radiative Properties of Hot Dense Matter*, edited by W. H. Goldstein, C. Hopper, J. Gautier, J. Seely and R. Lee (World Scientific, Singapore, 1990).
- [3] A. Bar-Shalom, J. Oreg, and W.H. Goldstein, in *Atomic Processes in Plasmas*, edited by E. S. Marmor and J. L. Terry, AIP Conf. Proc. No. 257 (AIP, New York, 1991).
- [4] A. Bar-Shalom, J. Oreg, and W. H. Goldstein, *J. Quantum Spectrosc. Radiat. Transfer* **51**, 27 (1994).
- [5] A. Bar-Shalom, J. Oreg, and W.H. Goldstein, *Phys. Rev. E* **51**, 4882 (1995).
- [6] J. F. Seely *et al.* *J. Quantum Spectrosc. Radiat. Transfer* **51**, 349 (1994).
- [7] J. D. Bauer *et al.* *Phys. Rev. E* (to be published).
- [8] D. R. Kania *et al.*, *Phys. Rev. A* **46**, 7853 (1992).
- [9] C. Bauche-Arnoult, J. Bauche, and M. Klapisch, *Phys. Rev. A* **25**, 2641 (1982).
- [10] C. Bauche-Arnoult, J. Bauche, and M. Klapisch, *Phys. Rev. A* **31**, 2248 (1995).
- [11] A. Bar-Shalom, J. Oreg, and W. H. Goldstein, *J. Quant. Spectrosc. Radiat. Transfer* **51**, 27 (1994).